Comparison of coupled solute flux through sodium- and enhanced-bentonite barriers leveraging two decades of experimental data

Kristin Sample-Lord [i)], Gretchen Bohnhoff [ii)], Joseph Scalia [iii)] and Michael Malusis [iv)]

i) Assistant Professor, Civil and Environmental Engineering, Villanova University, 800 Lancaster Ave., Villanova, PA 19073, USA.
ii) Associate Professor, Department of Civil & Environmental Engineering, University of Wisconsin-Platteville, Platteville, WI, USA.
iii) Assistant Professor, Department of Civil & Environmental Engineering, Colorado State University, Fort Collins, CO, USA.
iv) Professor, Department of Civil & Environmental Engineering, Bucknell University, Lewisburg, PA, USA.

ABSTRACT

Enhanced bentonites (EBs) developed for improved hydraulic compatibility (i.e., low hydraulic conductivity, k, to chemical solutions) relative to unamended sodium bentonite (NaB) are increasingly being used in geosynthetic clay liners (GCLs). Both NaB and EBs have been shown to exhibit semipermeable membrane behavior. Thus, predictions of barrier performance for different bentonites that focus only on advection and ignore the influence of membrane behavior and diffusion on solute flux are inaccurate. In this paper, data from solute transport studies conducted over the last 20 years were used to compare expected solute flux through NaB and EB barriers with and without accounting for membrane behavior. Coupled effective diffusion coefficients (D^*), membrane efficiency coefficients (ω), and k values for NaBs and EBs from the literature were used with an analytical solution for coupled solute transport to predict dimensionless transient and steady-state solute fluxes exiting the barrier (J^*_j and J^*_{ss}) under typical GCL boundary conditions. Values of J^*_j and J^*_{ss} for a range of salt solutions were compared for NaB GCLs and five different EBs. For a given source concentration (C_o) of a given salt, EBs generally exhibit lower k, higher ω, and similar D^* relative to NaB GCLs. As a result, J^*_{ss} values for EBs were 10–60% lower relative to NaB for monovalent (KCl, NaCl) solutions and up to 95% lower relative to NaB for divalent ($CaCl_2$) solutions. The bentonites with the highest ω, but not necessarily the lowest k, correlated to the lowest J^*_{ss} for all solutions.

Keywords: anion exclusion, diffusion, geosynthetic clay liner, membrane behavior

1 INTRODUCTION

Bentonite commonly is used in geoenvironmental containment barriers, including geosynthetic clay liners (GCLs). Waste containment regulations typically require that bentonite barriers exhibit low hydraulic conductivity, k, to water (e.g., $k < 10^{-9}$ m/s; Rowe, 1987; Shackelford, 1991) to limit advective flux. Consideration of diffusion coefficients is not a regulatory requirement for most GCL applications, even though diffusion becomes a significant to dominant transport mechanism when advection is restricted at $k < 10^{-10}$ m/s (e.g., Rowe et al., 1988; Lake and Rowe, 2000; Rowe et al., 2004; Lange et al., 2009; Shackelford, 2014). In addition, although bentonite barriers have been shown to exhibit semipermeable membrane behavior that could result in significant reductions of total flux, the importance of accurately accounting for membrane behavior in transport predictions still is not well understood. Thus, predictions of long-term (steady-state) total flux through GCLs and other bentonite barriers typically neglect coupled membrane behavior and diffusion effects, resulting in inaccurate predictions of containment performance. This knowledge gap has motivated an increase in experimental studies focused on measurement of membrane behavior and diffusion properties of GCLs and Na-bentonite (NaB) over the last two decades.

Due to chemical incompatibility issues exhibited by NaB GCLs, there also has been a rapid increase in the development of enhanced bentonite (EB) GCLs. Bentonite-polymer composite (BPC), multi-swellable bentonite (MSB), HYPER clay, and dense-prehydrated (DPH) GCLs have been shown to exhibit enhanced hydraulic properties (lower k) and resistance to chemical incompatibility, relative to NaB GCLs (see Scalia et al. 2018). However, there has been substantially less research regarding the relevance of diffusion and membrane behavior for EB GCLs and implications for relative long-term performance compared to NaB GCLs. Initial research to date indicates that EB GCLs exhibit significant membrane behavior, similar to (if not more so) than NaB GCLs. In this paper, data from two decades of experimental literature were combined with an established theoretical framework for coupled solute transport through clay membranes to provide further assessment of the relative role of coupled phenomena in NaB and EB GCL barriers.

2 SUMMARY OF EXPERIMENTAL DATA

Membrane behavior in bentonite results in restricted solute migration as a result of hyperfiltration, chemico-osmotic counter advection, and restricted diffusion (Malusis et al., 2003). Membrane behavior is quantified using the membrane efficiency coefficient, ω, which varies between zero (no membrane behavior) and unity (perfect membrane, i.e., $0 \leq \omega \leq 1$). Reductions in solute diffusion coefficients have been shown to correlate with increases in membrane behavior for NaB and EB barriers (e.g., Malusis and Shackelford, 2002a; Bohnhoff and Shackelford, 2015; Dominijanni et al., 2018).

Membrane efficiency typically is measured using a closed-system testing apparatus, as described by Malusis et al. (2001). In general, a specimen is confined in a cell and salt solution of a particular source concentration (C_o) is circulated across the top boundary of the specimen while deionized water (DIW) is circulated across the bottom boundary. Since the system is "closed", no liquid flow is allowed to occur through the specimen and a pressure builds up on the high concentration side of the specimen to counteract chemico-osmotic counterflow. The hydraulic pressure difference across the specimen, ΔP, is compared to the osmotic pressure difference, $\Delta\pi$, which corresponds to the theoretical maximum value of ΔP for an ideal semipermeable membrane, to calculate the chemico-osmotic efficiency coefficient, ω (i.e., $\omega = \Delta P / \Delta\pi$). Simultaneously, solutes diffuse through the specimen from the top to the bottom boundary due to the applied concentration gradient. For each concentration stage, coupled effective diffusion coefficients (D^*) can be determined using the steady-state through-diffusion analysis method described in Shackelford (1991).

Tables 1 and 2 and Figures 1a,b represent a compilation of data from experimental literature over the last two decades whereby membrane behavior and diffusion testing was performed using the described test methods (i.e., closed-system apparatus circulating simple salt solutions and performed to steady-state conditions). All of the studies used similar simple salt solutions (KCl, NaCl, or $CaCl_2$) and concentration ranges (< 0.4 M). With the exception of one study in Table 1 (Malusis and Shackelford, 2002b), all of the studies reported D^* for Cl^- in addition to ω for each concentration stage. As shown in Table 2, very limited data is available for membrane and diffusion behavior of NaBs and EBs for $CaCl_2$ solutions. The data in Tables 1 and 2 are represented visually in Figures 1a,b. More in-depth analysis comparing transport properties of different EBs is available in Scalia et al. (2018).

Values of k also are included in Tables 1 and 2, solely for use in the coupled solute transport analysis described later. When values of k were not reported for specific source concentrations in the membrane behavior studies, k values were assumed from other sources in the literature, as described in the notes of Tables 1 and 2.

Table 1. Experimental data from the membrane behavior and diffusion literature for sodium and enhanced bentonites tested with **monovalent (KCl and NaCl)** salt solutions.

Ref.	Material Tested	Salt	Source concentration, C_o (mM)	Coupled effective diffusion coefficient, D^* for Cl^- (m^2/s)	Membrane efficiency coefficient, ω (-)	Hydraulic conductivity, k (m/s)	Porosity, n (-)
1	NaB GCL	KCl	3.9	7.05×10^{-11}	0.63	1.65×10^{-11}	0.80
			8.7	1.16×10^{-10}	0.49	1.33×10^{-11}	0.79
			20	2.14×10^{-10}	0.32	2.06×10^{-11}	0.79
			47	2.34×10^{-10}	0.14	1.48×10^{-11}	0.78
			3.9	-	0.69	3.86×10^{-12} *	0.74
			6	-	0.58	3.86×10^{-12} *	0.74
			8.7	-	0.53	3.86×10^{-12} *	0.74
			20	-	0.32	3.86×10^{-12} *	0.74
			47	-	0.16	6.24×10^{-12}	0.74
			3.9	-	0.52	2.98×10^{-11} *	0.86
			6	-	0.42	2.98×10^{-11} *	0.86
			8.7	-	0.42	2.98×10^{-11} *	0.86
			20	-	0.26	2.98×10^{-11} *	0.86
			47	-	0.08	4.74×10^{-11}	0.86
2	NaB GCL	KCl	3.9	1.26×10^{-10}	0.561	3.06×10^{-11}	0.80
			6	1.66×10^{-10}	0.418	3.06×10^{-11}	0.80
			8.7	2.08×10^{-10}	0.286	3.06×10^{-11}	0.79
			20	2.69×10^{-10}	0.076	3.06×10^{-11}	0.79
			47	2.79×10^{-10}	0.015	3.06×10^{-11}	0.79
3	NaB GCL	KCl	21.1	1.11×10^{-10}	0.097	2.06×10^{-11} *	0.79
			35.2	1.35×10^{-10}	0.054	2.06×10^{-11} *	0.79
			54.9	1.47×10^{-10}	0.034	1.48×10^{-11} *	0.79
			108	1.52×10^{-10}	0.015	1.48×10^{-11} *	0.79
			240	1.65×10^{-10}	0.004	1.48×10^{-11} *	0.79
			408	1.83×10^{-10}	0	1.48×10^{-11} *	0.79
4	NaB GCL	NaCl	5.16	-	0.68	8.00×10^{-12} *	0.81
			10.27	2.54×10^{-10}	0.58	8.00×10^{-12} *	0.81
			20.24	3.52×10^{-10}	0.33	8.00×10^{-12} *	0.81
			51.94	4.19×10^{-10}	0.14	8.00×10^{-12} *	0.81
			109.31	4.60×10^{-10}	0.05	8.00×10^{-12} *	0.81
5	Homo NaB	KCl	19	1.80×10^{-10}	0.61	7.50×10^{-12} *	0.87
			30	3.10×10^{-10}	0.42	7.50×10^{-12} *	0.87
			49	4.10×10^{-10}	0.31	7.50×10^{-12} *	0.87
6	DPH-GCL	KCl	8.7	3.90×10^{-11}	0.73	1.80×10^{-12}	0.53
			20	4.50×10^{-11}	0.57	1.30×10^{-12}	0.64
			47	7.50×10^{-11}	0.26	1.90×10^{-12}	0.60
			80	6.50×10^{-11}	0.25	1.00×10^{-12}	0.63
			160	9.20×10^{-11}	0.15	1.20×10^{-12}	0.62
7	BPC	KCl	4.7	1.00×10^{-10}	0.8	6.20×10^{-12} *	0.92
			9.3	1.48×10^{-10}	0.65	6.20×10^{-12} *	0.92
			20	1.39×10^{-10}	0.43	6.20×10^{-12} *	0.92
			54	2.22×10^{-10}	0.17	6.20×10^{-12} *	0.92
			4.7	3.66×10^{-11}	0.88	6.20×10^{-12} *	0.80
			9.3	5.52×10^{-11}	0.73	6.20×10^{-12} *	0.80
			20	6.77×10^{-11}	0.46	6.20×10^{-12} *	0.80
			54	1.03×10^{-10}	0.2	6.20×10^{-12} *	0.80
			4.7	1.70×10^{-10}	0.55	6.20×10^{-12} *	0.95
			9.3	2.24×10^{-10}	0.32	6.20×10^{-12} *	0.95
			20	2.72×10^{-10}	0.14	6.20×10^{-12} *	0.95
			54	2.90×10^{-10}	0.04	6.20×10^{-12} *	0.95
			4.7	7.33×10^{-11}	0.46	6.20×10^{-12} *	0.84
			9.3	9.87×10^{-11}	0.38	6.20×10^{-12} *	0.84
			20	1.37×10^{-10}	0.25	6.20×10^{-12} *	0.84
			54	1.58×10^{-10}	0.1	6.20×10^{-12} *	0.84

References:
1 = Malusis & Shackelford (2002a,b); *for tap water
2 = Kang & Shackelford (2011)/Malusis et al. (2015)
3 = Shackelford et al. (2016); * Malusis & Shackelford (2002a,b)
4 = Dominjanni et al. (2013); *for DI water
5 = Sample-Lord (2015); * for DI water
6 = Malusis & Daniyarov (2016)
7 = Bohnhoff & Shackelford (2015); * Scalia (2012) for DI water

Table 2. Experimental data from the membrane behavior and diffusion literature for sodium and enhanced bentonites tested with **divalent ($CaCl_2$)** salt solutions.

Ref.	Material Tested	Salt	Source concentration, C_o (mM)	Coupled effective diffusion coefficient, D^* for Cl^- (m^2/s)	Membrane efficiency coefficient, ω (-)	Hydraulic conductivity, k (m/s)	Porosity, n (-)
8	NaB GCL	$CaCl_2$	5	1.21×10^{-10}	0	1.50×10^{-10} *	0.718
9	NaB	$CaCl_2$	1	4.00×10^{-11}	0.29	6.42×10^{-12} *	0.718
			5	2.22×10^{-10}	0	4.02×10^{-11} *	0.718
10	BPC	$CaCl_2$	5	3.30×10^{-11}	0.95	2.08×10^{-11} *	0.87
			10	9.40×10^{-11}	0	2.08×10^{-11} *	0.87
			5	9.80×10^{-12}	0.39	2.08×10^{-11} *	0.94
			10	2.10×10^{-11}	0.11	2.08×10^{-11} *	0.94
			20	4.30×10^{-11}	0	3.90×10^{-11} *	0.94
9	MSB	$CaCl_2$	5	1.79×10^{-10}	0	6.00×10^{-11} *	0.718
9	Hyper Clay	$CaCl_2$	1	4.40×10^{-11}	0.65	6.50×10^{-12} *	0.718
			5	1.67×10^{-10}	0.13	3.10×10^{-12} *	0.718

References:
8 = Shackelford & Lee (2003); * Jo et al. (2005)
9 = Di Emidio (2015); * Mazzieri and Pasqualini (2006)
10 = Bohnhoff et al. (2014); * Scalia et al. (2014), assumed k for 5 mM ≈ 10 mM

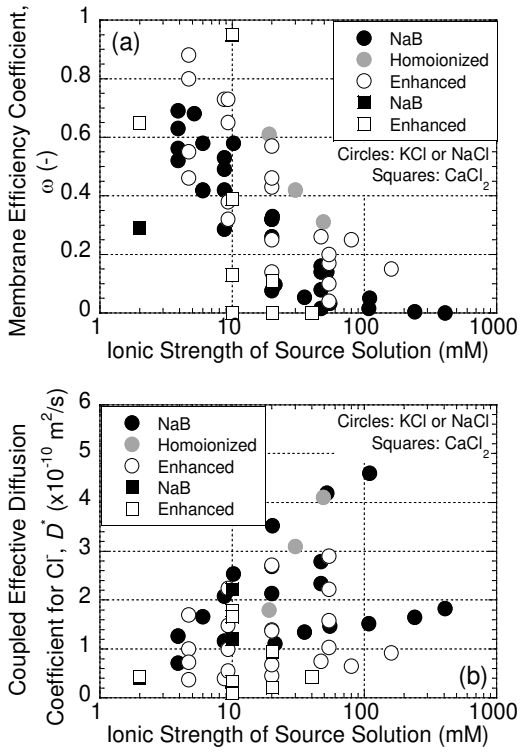

Fig. 1. Summary of data from the experimental literature for sodium and enhanced bentonites: (a) membrane efficiency coefficients; and (b) coupled effective diffusion coefficients for chloride (Cl^-) as a function of ionic strength of the source solution.

As shown in Figure 1a, both NaB and EBs have been shown to exhibit membrane behavior, with values of ω generally decreasing with increasing ionic strength. EBs (open symbols in Fig. 1a) tend to exhibit the highest values of ω (e.g., ω > 0.7) relative to NaBs, and membrane behavior continues to persist in EBs at concentrations that destroy significant membrane behavior in most NaBs. The general observation that ω is higher for EB GCLs than NaB GCLs at similar porosities (n) and C_o was reported in Scalia et al. (2018).

From the membrane behavior studies in Table 1 that also reported D^* for chloride (Cl^-), the values of D^* as a function of source solution ionic strength are summarized in Fig. 1b. As expected, D^* for Cl^- for EBs was generally lower than NaB, which may be due in part to membrane behavior effects. Values of D^* for Cl^- are plotted against the corresponding values of ω (i.e., measured in the same test and concentration stage) in Figs 2a,b. The inverse relationships between D^* and ω for both NaBs and EBs in Fig. 2 demonstrate the significant effect of membrane behavior on expected diffusive solute flux through GCLs and other bentonite barriers. Assessment of the data in Tables 1 and 2 and Figures 1 and 2 also suggests that consideration of coupled solute flux in transport analyses may become even more important with the continued development and adoption of novel bentonites that exhibit higher ω.

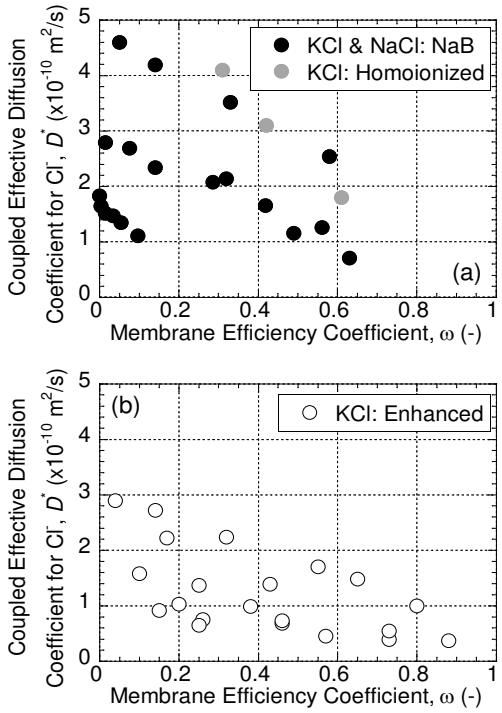

Fig. 2. Relationship between measured coupled effective diffusion coefficients for chloride and membrane behavior efficiencies from the literature for (a) sodium and sodium homo-ionized bentonite, and (b) enhanced bentonite.

3 COUPLED SOLUTE FLUX ANALYSIS

Previously established theoretical frameworks for coupled solute transport through clay membranes allow for prediction of solute flux through GCLs for single-salt solutions with consideration of membrane behavior effects (e.g., Manassero and Dominijanni, 2003; Malusis et al., 2012; Dominijanni et al., 2013). However,

assumption of representative values of k, D^* and ω within these models can be challenging, due to the dynamic and coupled nature of bentonite properties that depend on solution chemistry, degree of saturation, void ratio, fabric changes, and so on. In addition, current understanding of membrane behavior and diffusion in EBs is limited, partly due to the recent emergence and increased adoption of EB GCLs. The analysis presented herein leveraged experimental ω and D^* data from the last two decades summarized in Tables 1 and 2 to predict and compare transient and steady-state coupled solute flux (J^*_j and J^*_{ss}) for different NaB GCLs and EB GCLs. Values of J^*_j and J^*_{ss} for NaB GCLs and EB GCLs were determined with an analytical solution and compared for a range of monovalent (KCl, NaCl) and divalent ($CaCl_2$) salt concentrations, as described subsequently.

Total flux of solute j (J_j) through a clay membrane, in the absence of an applied electrical gradient, can be written as (Malusis et al., 2012):

$$J_j = J_{ha} + J_\pi + J_d \tag{1}$$

where J_{ha} is advective solute flux (which includes a solute rejection factor of 1-ω to account for hyperfiltration effects; Saindon and Whitworth, 2005), J_π is chemico-osmotic counter-advection, and J_d is diffusive flux. Directions of the flux components for a typical GCL containment scenario are shown in Fig. 3.

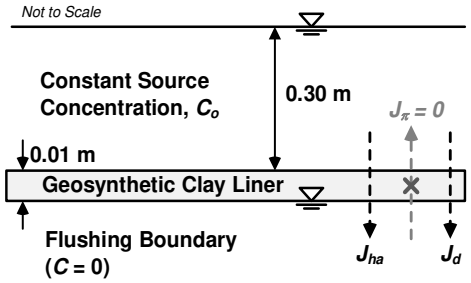

Fig. 3. Assumed conditions for the steady-state flux analysis.

The coupled solute flux exiting the barrier was determined for NaB GCLs and EB GCLs based on the following analytical solution for the scenario shown in Fig. 3:

$$J^*_j = (1-\omega)\exp\left(\frac{P_{eg}}{2}\right)\left\{\frac{P_{eg}}{2\sinh\left(P_{eg}/2\right)} + 2\pi^2\sum_{m=1}^{\infty}\frac{-1^m m^2}{\left(P_{eg}{}^2/4\right)+m^2\pi^2}\exp\left[\left(-\frac{P_{eg}{}^2}{4}-(1-\omega)m^2\pi^2\right)T^*\right]\right\} \tag{2}$$

where J^*_j is the dimensionless flux of solute (see Malusis et al., 2018), T^* is the dimensionless time factor, and P_{eg} is the global Peclet number. The parameters T^* and P_{eg} are defined as follows:

$$T^* = \frac{D_{se}t}{L^2}, \qquad P_{eg} = -\frac{kL}{nD_{se}\gamma_w}\frac{\Delta P}{\Delta x} \tag{3}$$

where t is time, L is the thickness of the barrier, γ_w is the unit weight of liquid (water), D_{se} is the effective diffusion coefficient ($D_{se}=\tau_m D_{so}$, where τ_m=matrix tortuosity factor and D_{so}=free-solution diffusion coefficient; alternatively D_{se} can also be assumed to be $=D^*/(1-\omega)$), ΔP is the boundary pressure difference, and Δx is the change in distance ($x = L$ for this analysis). Equation 2 is an analytical solution from Rabideau and Khandelwal (1998), modified for cases in which $\omega > 0$, but the effect of chemico-osmotic counter flow on J^*_j is negligible (Malusis et al., 2018). The solution in Eq. 2 also was used to determine J^*_j at high T^*, at which the J^*_j value becomes steady and represents J^*_{ss}.

The following assumptions are included in the use of Eq. 2 for one-dimensional solute transport through a clay membrane in contact with a constant, single-salt source solution: (1) the solution is sufficiently dilute for ideal relationships to be valid; (2) the term 1-ω is a reasonable approximation for restrictive tortuosity for clay membranes (Manassero and Dominijanni, 2003); (3) ω is constant for a given C_o and does not vary spatially (i.e., ω values used were the "global" ω values); and (4) the effect of chemico-osmotic counter flow on J^*_{ss} is negligible. Malusis et al. (2018) concluded that at low values of P_e (e.g., $P_e < 0.01$, as in this study), the percentage reduction in solute flux due solely to chemico-osmotic counter-advection is only 0.5 – 10 % for all values of ω. The following assumptions were made regarding the GCL under steady-state conditions (see Fig. 3): (1) the height of the ponded leachate above the GCL was 0.3 m; (2) the GCL was 0.01-m thick; (3) the concentration at the top boundary is the constant salt source concentration C_o; and (4) the bottom boundary is perfectly flushing.

4 COMPARISON OF MATERIAL TYPES

Based on the transport properties reported in Tables 1 and 2, Figure 4a,b compares the predicted J^*_j for NaB and EB GCLs for the same C_o (20 mM KCl and 5 mM $CaCl_2$). Figure 5a,b shows a side-by-side comparison of the transport property values and the corresponding long-term performance as predicted from J^*_{ss} for the same C_o. For purposes of this simple comparison, results from specimens with very high porosities (i.e., the BPC specimens that had $n > 0.9$) were not included. As shown in Fig. 5a, for a given C_o (20 mM KCl), the enhanced and treated bentonites (i.e, BPC, DPH-GCL, and homoionized NaB) generally have lower k, higher ω, and similar D^* values compared to those reported for NaB GCLs. Thus, J^*_j and J^*_{ss} values were lower for GCLs based on enhanced and treated bentonite properties, relative to NaB GCLs (Figs. 4 and 5). For example, for C_o = 20 mM KCl, the average J^*_{ss} for NaB GCLs was 0.84, compared to only 0.43 for DPH and 0.65 for BPC.

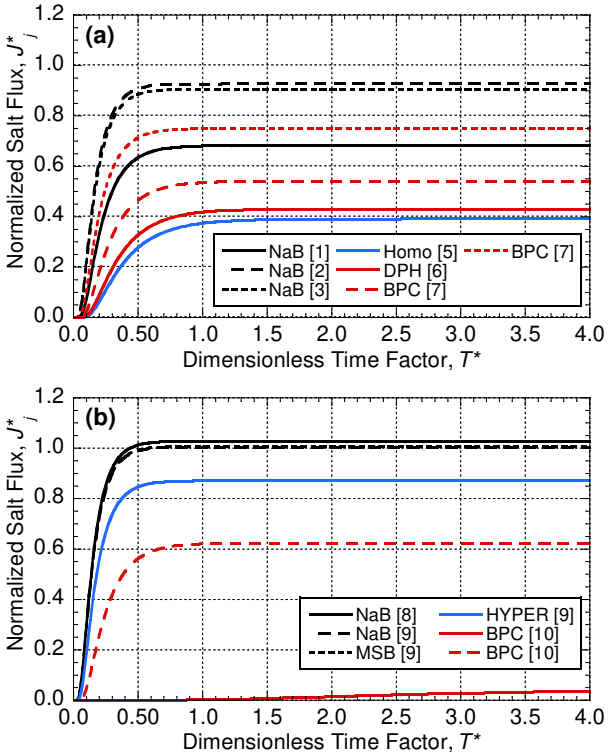

Fig. 4. Comparison of dimensionless solute flux (J^*_j) for NaB and EB GCLs for source concentrations of (a) 20 mM KCl and (b) 5 mM $CaCl_2$ [Bracketed numbers in legend correlate to numbered references in Tables 1 and 2].

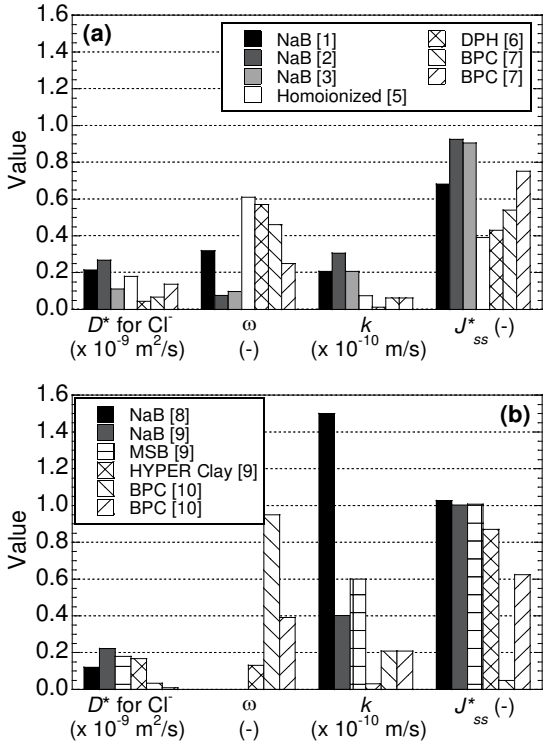

Fig. 5. Side-by-side comparisons of hydraulic conductivities (k), coupled effective diffusion coefficients (D^*), membrane efficiencies (ω), and corresponding predicted steady-state solute fluxes (J^*_{ss}) for NaB and EB GCLs for source concentrations (C_o) of (a) 20 mM KCl and (b) 5 mM $CaCl_2$.

Similarly, based on the limited literature available for $CaCl_2$ solutions EBs (MSB, Hyper clay, BPC) exhibit substantially lower k (e.g. > 1 order of magnitude lower), higher ω, and similar D^* values compared to those reported for NaB GCLs resulting in generally lower J^*_j and J^*_{ss} relative to NaB GCLs. For C_o = 5 mM $CaCl_2$, J^*_{ss} was ~1.0 for the NaB GCLs and 0.05 to 0.62 for the BPC. However, there is no ω data for EBs at C_o > 20 mM $CaCl_2$. Membrane behavior often is destroyed for NaB and EBs at C_o > 10 mM $CaCl_2$.

Overall, the results in Figs. 5a,b indicate that the materials with the highest ω, and not necessarily just the lowest k, correlated to the lowest values of J^*_{ss} (i.e., provide the best predicted barrier performance). These results emphasize the importance of considering membrane behavior effects, in addition to hydraulic performance, when comparing J^*_{ss} for different bentonite-based barrier materials.

Comparison of the predicted J^*_{ss} across a GCL for different NaBs and EBs for a range of monovalent salt concentrations (KCl and NaCl) parameterized with experimental data in Table 1 is shown in Fig. 6. Only results for monovalent salt solutions are included in Fig. 6 due to the very limited data available for $CaCl_2$. The J^*_{ss} for all NaB and EBs increases with increasing C_o as would be expected due to decreases in ω and increases in D^* with increasing concentration.

Some of the k values presented in Table 1 and used for determining J^*_{ss} in Fig. 6 had to be assumed from other sources of literature or for different source concentrations (see Table 1 notes). These k assumptions potentially may have dampened the difference between predicted J^*_{ss} for EBs versus NaBs and the predicted increases in J^*_{ss} with increasing C_o. However, since Fig. 6 only represents predictions of J^*_{ss} for monovalent salt solutions at concentrations less than 0.5 M, k is not expected to increase substantially with increasing C_o (i.e., relative to $CaCl_2$ solutions; Shackelford et al., 2000; Scalia et al., 2018). Apart from the BPC with the highest porosity (n = 0.95), EB GCLs generally correlate with lower predicted J^*_{ss} than NaB GCLs for a given salt solution. This observation suggests EBs may provide not only superior hydraulic performance, but also better overall long-term containment when coupled phenomena and diffusion are considered.

To evaluate the impact of including ω in J^*_{ss} predictions, the percent error was calculated for scenarios where values of ω were assumed to be zero in Eq. 2 (i.e., % error = 100 % x $[J^*_{ss} - J^*_{ss(\omega=0)}] / J^*_{ss}$). This analysis was completed for the same concentrations of KCl and $CaCl_2$ as presented in Figs. 4 and 5 (i.e., 20 mM KCl and 5 mM $CaCl_2$) and the results are presented in Fig. 7a,b. The impact of ignoring ω is significantly higher for EBs compared to NaB for both KCl and $CaCl_2$ and is more pronounced for $CaCl_2$. For example, the percent error for NaB and BPC with 20 mM KCl is 8 – 47 % and 33 – 133 %, respectively.

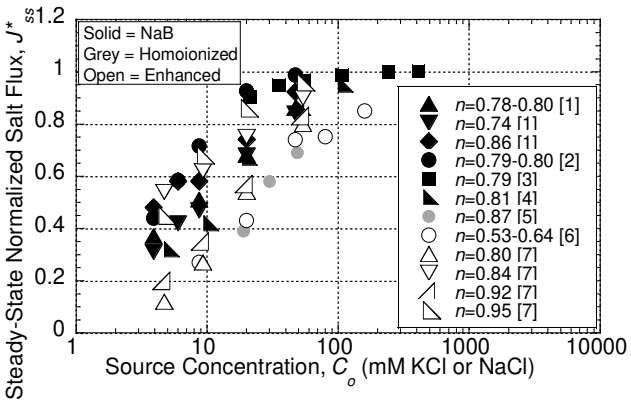

Fig. 6. Predicted steady-state normalized solute flux across a GCL for different NaB and EBs as a function of source KCl or NaCl concentration [Bracketed numbers in legend correlate to numbered references in Table 1].

An important caveat to the results in Fig. 7a is that these error ranges for NaB represent an extreme case, i.e., for a low concentration, monovalent salt solution where the NaB still exhibits low k and measurable ω. For more aggressive solutions or after exposure to field conditions that can degrade NaB GCLs (e.g., cation exchange, desiccation cycles), impacts of membrane behavior on J^*_{ss} likely would diminish due to decreases in ω, and hydraulic flux likely would become the dominant transport mechanism.

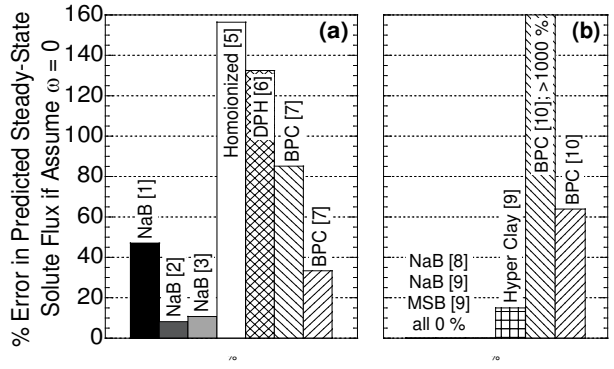

Fig. 7. Percent difference in predicted steady-state solute flux when assuming ω = 0 (% difference = 100 % x $[J^*_{ss} - J^*_{ss(\omega=0)}]$ / J^*_{ss}) for (a) C_o = 20 mM KCl, and (b) C_o = 5 mM $CaCl_2$.

For example, the percent error in Fig. 7b for NaB becomes zero, due to the destruction of membrane behavior by the $CaCl_2$ solution. In contrast, ω continues to play an important role in J^*_{ss} for BPC for the $CaCl_2$ solution (Fig. 7b), suggesting inclusion of ω in coupled solute flux predictions is even more important for EB GCLs than NaB GCLs.

5 CONCLUSIONS

Data from experimental solute transport studies conducted over the last twenty years were used in an analytical solution for coupled transport to predict transient and steady-state solute flux (J^*_j and J^*_{ss}) exiting a geosynthetic clay liner (GCL). Values of J^*_{ss} through NaB and EB GCLs were compared with and without accounting for membrane behavior. Results indicate that EB GCLs may provide not only superior hydraulic performance, but also better overall long-term containment when coupled phenomena and diffusion are considered. In addition, inclusion of membrane efficiency coefficients (ω) is especially important for solute flux predictions for EB GCLs as the bentonites with the highest ω, but not necessarily the lowest k, correlated to the lowest J^*_{ss} for all solutions included in the analysis.

REFERENCES

1) Bohnhoff, G. and Shackelford, C. (2015): Salt diffusion through a bentonite-polymer composite, *Clays and Clay Minerals*, 63(3) 145-162.
2) Bohnhoff, G., Sample-Lord, K. and Shackelford, C. (2014): Calcium-resistant membrane behavior of polymerized bentonite, *Journal of Geotechnical and Geoenvironmental Engineering*, 140(3).
3) Di Emidio, G., Mazzieri, F., Verastegui-Flores, R., Van Impe, W. and Bezuijen, A. (2015): Polymer-treated bentonite clay for chemical-resistant geosynthetic clay liners, *Geosynthetics International*, 22 (1), 125-137.
4) Dominijanni, A., Guarena, N. and Manassero, M. (2018): Laboratory assessment of semipermeable properties of a natural sodium bentonite, *Canadian Geotechnical Journal*, 55(11), 1611-1631. doi:10.1139/cgj-2017-0599
5) Dominijanni, A., Manassero, M. and Puma, S. (2013): Coupled chemical-hydraulic-mechanical behaviour of bentonites, *Geotechnique*, 63, 191-205.
6) Jo, H., Benson, C., Shackelford, C., Lee, J-M. and Edil, T. (2005): Long-term hydraulic conductivity of a geosynthetic clay liner permeated with inorganic salt solutions, *Journal of Geotechnical and Geoenvironmental Engineering*, 131(4), 405-417.
7) Kang, J. B., and Shackelford, C. D. (2011). Consolidation enhanced membrane behavior of a geosynthetic clay liner, *Geotextiles and Geomembranes*, 29(6), 544–556.
8) Lake, C. and Rowe, R. (2000): Diffusion of sodium and chloride through geosynthetic clay liners, *Geotextiles and Geomembranes*, 18, 101–131.
9) Lange, K., Rowe, R. and Jamieson, H. (2009): Diffusion of metals in geosynthetic clay liners, *Geosynthetics International*, 16(1), 11–27.
10) Malusis, M. and Daniyarov, A. (2016): Membrane efficiency and diffusive tortuosity of a dense prehydrated geosynthetic clay liner, *Geotextiles and Geomembranes*, 44(5), 719-730.
11) Malusis, M. and Shackelford, C. (2002a): Coupling effects during steady-state solute diffusion through a semipermeable clay membrane, *Environmental Science and Technology*, 36(6), 1312-1319.
12) Malusis, M. and Shackelford, C. (2002b): Chemico-osmotic efficiency of a geosynthetic clay liner, *Journal of Geotechnical and Geoenvironmental Engineering*, 128(2), 97-106.
13) Malusis, M., Shackelford, C. and Maneval, J. (2012): Critical review of coupled flux formulations for clay membranes based on nonequilibrium thermodynamics, *Journal of Contaminant Hydrology*, 138-139, 40-59.
14) Malusis, M., Shackelford, C. and Olsen, H. W. (2001): A laboratory apparatus to measure chemico-osmotic efficiency coefficients for clay soils, *Geotechnical Testing Journal*, 24(3),

229–242.
15) Malusis, M., Shackelford, C. and Olsen, H. (2003): Flow and transport through clay membrane barriers, *Engineering Geology*, 70(2-3), 235-248.
16) Malusis, M., Kang, J. and Shackelford, C. (2015): Restricted salt diffusion in a geosynthetic clay liner, *Environmental Geotechnics*, 2(2), 68-77.
17) Malusis, M., Scalia, J., Norris, A. and Shackelford, C. (2018): Effect of chemico-osmosis on solute transport in clay barriers, *Environmental Geotechnics*, online ahead of print, 1-10. https://doi.org/10.1680/jenge.17.00109.
18) Manassero, M. and Dominijanni, A. (2003): Modelling the osmosis effect on solute migration through porous media, *Geotechnique*, 53, 481-492.
19) Mazzieri, F. and Pasqualini, E. (2006): Evaluating the permeability of an organically modified bentonite to natural seawater, *Proceedings of the 5th ICEG Environmental Geotechnics*, Thomas Telford, London, pp. 749 - 756.
20) Rabideau, A. and Khandelwal, A. (1998): Boundary conditions for modeling transport in vertical barriers, *Journal of Environmental Engineering*, 124(11), 1135-1139.
21) Rowe, R. (1987): Pollutant transport through barriers. Geotechnical practice for waste disposal, *Special Publication No. 13*, R. Woods, Ed., ASCE, New York, NY, 159-1815.
22) Rowe, R., Caers, C. and Barone, F. (1988): Laboratory determination of diffusion and distribution coefficients of contaminants using undisturbed clayey soil, *Canadian Geotechnical Journal*, 25(1): 108-1185.
23) Rowe, R., Quigley, R., Brachman, R. and Booker, J. (2004): *Barrier Systems for Waste Disposal Facilities*, Taylor & Francis, London.
24) Saindon, R. and Whitworth, T. (2005): Hyperfiltration of NaCl solutions using a simulated clay/sand mixture at low compaction pressures, *Aquatic Geochemistry*, 11, 433-444.
25) Sample-Lord, K. (2015): Membrane Behavior and Diffusion in Unsaturated Sodium Bentonite, Ph.D. Dissertation, Colorado State University, Fort Collins, Colorado, USA
26) Scalia, J. (2012): Bentonite-polymer composites for containment applications, Ph.D. dissertation, Univ. of Wisconsin–Madison, Madison, WI.
27) Scalia, J., Benson, C.H., Bohnhoff, G.L, Edil, T. and Shackelford, C.D. (2014): Long-term hydraulic conductivity of a bentonite-polymer composite permeated with aggressive inorganic solutions, *Journal of Geotechnical and Geoenvironmental Engineering*, 140, 04013025-1-13.
28) Scalia, J., Bohnhoff, G., Shackelford, C., Benson, C., Sample-Lord, K., Malusis, M. and Likos, W. (2018): Enhanced bentonites for containment of inorganic waste leachates by GCLs, *Geosynthetics International*, 25(4), 392-411.
29) Shackelford, C. (1991): Laboratory diffusion testing for waste disposal - A review, *Journal of Contaminant Hydrology,* 7(3), 177–217.
30) Shackelford, C. (2014): The ISSMGE Kerry Rowe Lecture: The role of diffusion in environmental geotechnics, *Canadian Geotechnical Journal*, 51(11), 1219–1242.
31) Shackelford C., Meier, A. and Sample-Lord, K. (2016): Limiting membrane and diffusion behavior of a geosynthetic clay liner, *Geotextiles and Geomembranes*, 44(5), 707-718.
32) Shackelford, C. and Lee, J. (2003): The destructive role of diffusion on clay membrane behavior. *Clays and Clay Minerals*, 51(2), 186-196.